

Epithelial Wntless (Wls) regulates postnatal alveologenesis

Yinshan Fang¹, Hongxia Shao^{1,2}, Qi Wu², Neng Chun Wong¹, Natalie Tsong¹,

Patricia Sime³, Jianwen Que^{1*}

1. Division of Digestive and Liver Diseases, Department of Medicine, USA; Columbia Center for Human Development, Columbia University Medical Center, New York, NY 10032, USA.

2. Tianjin Haihe Hospital, Tianjin, Tianjin 300350, China.

3. Department of Internal Medicine, Virginia Commonwealth University in Richmond, Richmond, VA 23298, USA.

* Corresponding author: Jianwen Que, Center for Human Development, Columbia University Medical Center, BB-810, 650 West 168th Street, NY 10032, USA. E-mail: jq2240@cumc.columbia.edu.

Abstract

Alveologenesis requires the coordinated modulation of the epithelial and mesenchymal compartments to generate mature alveolar saccules for efficient gas exchange. However, the molecular mechanisms underlying the epithelial-mesenchymal interaction during alveologenesis are poorly understood. Here, we report that Wnts produced by epithelial cells are critical for neonatal alveologenesis. Deletion of the Wnt chaperon protein Wntless homolog (Wls) disrupts alveolar formation, resulting in enlarged saccules in *Sftpc-Cre/Nkx2.1-Cre; Wls^{loxP/loxP}* mutants. Although commitment of the alveolar epithelium is unaffected, α -SMA⁺ mesenchymal cells persist in the alveoli accompanied by increased collagen deposition and mutants exhibit exacerbated fibrosis following

bleomycin challenge. Notably, α -SMA⁺ cells include a significant number of endothelial cells resembling endothelial to mesenchymal transition (EndMT) which is also present in *Ager-CreER*; *Wls*^{loxp/loxp} mutants following early postnatal Wls deletion. These findings provide initial evidence that epithelial-derived Wnts are critical for the differentiation of the surrounding mesenchyme during early postnatal alveologenesis.

Introduction

Efficient gas exchange requires the coordinated development of the alveolar epithelium and mesenchyme during the neonatal stage (Hogan et al., 2014; Mund et al., 2008; Schittny et al., 2008; Yang et al., 2016). For example, mesenchymal cells differentiate into myofibroblasts (α -SMA⁺) which synergize with epithelial differentiation and subdivide saccules into alveoli (Bostrom et al., 1996; Chao et al., 2016; Lindahl et al., 1997). Meanwhile myofibroblasts produce the elastin-based extracellular matrix (ECM) to provide a complex and net-like structure for alveolar formation. The presence of myofibroblasts in interstitial regions is transient, present at around postnatal (P) day 3 to P14 in mice (McGowan et al., 2008). The persistent presence of myofibroblasts during the alveologenesis stage has been found in patients with bronchopulmonary dysplasia (BPD) which is characterized by alveolar simplification (Hilgendorff and O'Reilly, 2015; Husain et al., 1998; Jobe and Bancalari, 2001; Northway et al., 1967). In line with this, a hyperoxia-induced mouse model of BPD shows enrichment of myofibroblasts in the enlarged air sac post-alveologenesis (Branchfield et al., 2016). The epithelium seems to play an important role in the control of myofibroblasts during alveologenesis (Bourbon et al., 2005; Zhang et al., 2020). Consistently, loss of *Etv4/5* in epithelial cells leads to epithelial defects and increased expression of α -SMA in the simplified alveoli (Branchfield et al., 2016). However, it remains unknown what signal(s) from the epithelium are needed for regulating the transient presence of myofibroblasts.

Multiple signaling pathways including Wnt have been shown to regulate lung development (Bellusci et al., 1996; Colvin et al., 2001; Goss et al., 2009; Harris-Johnson et al., 2009; Kishimoto et al., 2020; Mucenski et al., 2003; Shu et al., 2005; Snowball et

al., 2015; Yin et al., 2008). Ablation of Wnt2/2b or the signaling mediator β -catenin results in the loss of lung progenitors and complete lung agenesis (Goss et al., 2009; Harris-Johnson et al., 2009). Moreover, overexpression of the Wnt inhibitor Dkk1 leads to disrupted proximal-distal patterning with proximalized lung epithelium in the distal domain (Shu et al., 2005). More recently, the protein Wntless homolog (Wls), a chaperon protein responsible for the transport and secretion of Wnt ligands, has been shown to regulate lung branching morphogenesis, epithelial differentiation and vascular development (Cornett et al., 2013; Jiang et al., 2013). However, in both studies *Shh-Cre* was used to delete *Wls* and mutants die at birth. Therefore, the function of Wls in postnatal lung development remains unclear.

Here, we use *Sftpc-Cre* and *Nkx2.1-Cre* mouse lines to delete *Wls* and observed BPD-like emphysema with severely enlarged saccules. Although epithelial commitment is not affected, extensive myofibroblasts persist in the adult mutant lungs with the presence of α -SMA⁺ endothelial cells. These mutants also display more severe pulmonary fibrosis than the controls following bleomycin challenge. Although neonatal deletion of *Wls* in the alveolar type II (AT2) cells with *Sftpc-CreER* does not impact homeostasis or exacerbate bleomycin-induced fibrosis, *Wls* ablation using *Ager-CreER* leads to the extensive presence of α -SMA⁺ endothelial cells.

Results and discussion

Deletion of epithelial *Wls* leads to enlarged air sacs with normal differentiation of AT1 and AT2 cells in *Sftpc-Cre*; *Wls*^{loxp/loxp} and *Nkx2.1-Cre*; *Wls*^{loxp/loxp} mutants.

Shh-Cre activities are detected in the early foregut at approximately embryonic (E) day 8.75 (Harris-Johnson et al., 2009; Rodriguez et al., 2010), prior to lung budding. The resultant *Shh-Cre*; *Wls*^{loxp/loxp} mutants succumbed to death at P0 (Jiang et al., 2013). We then used the transgenic *Sftpc-Cre* mouse line which is active at approximately E10.5 (Okubo and Hogan, 2004). Unlike *Shh-Cre*; *Wls*^{loxp/loxp} mutants, *Sftpc-Cre*; *Wls*^{loxp/loxp} mutants are viable and survive to adulthood. As expected, deletion of epithelial *Wls* leads to reduced Wnt signaling activities as evidenced by the *Axin2-LacZ* reporter allele at P30

(Fig. S1A). Histological examination reveals progressively enlarged air sac as observed in BPD patients and mouse models (Fig. 1A) (Hilgendorff and O'Reilly, 2015; Jobe and Bancalari, 2001). The mutant lungs exhibit normal alveologenesi s when examined at P0. However, air sac enlargement becomes apparent at P10 and more severe at P30, although proliferation and apoptosis are comparable with littermate controls (Fig. S1B-E). The numbers of alveolar saccules decrease from 209.67 ± 4.33 to 103.5 ± 5.9 per mm^2 ($p < 0.0001$) at P10, and 226.67 ± 3.71 to 73 ± 5.58 per mm^2 ($p < 0.0001$) at P30 (Fig. 1B). Conversely, the mean linear intercept (MLI) increases from $31.41 \pm 0.43 \mu\text{m}$ to $51.79 \pm 2.26 \mu\text{m}$ ($p < 0.001$) at P10, $26.83 \pm 1.08 \mu\text{m}$ to $62.86 \pm 2.51 \mu\text{m}$ ($p < 0.0001$) at P30 (Fig. 1C). These emphysema-like phenotypes remain in the adult mutant lungs (Fig. 1D). Similar enlarged air sacs are also present in the lungs of *Nkx2.1-Cre; Wls^{loxp/loxp}* mutants at P30 and P60 (Fig. 1E-H). Notably, the activities of the transgenic *Nkx2.1-Cre* can be detected starting at E10.5 in the embryonic lungs (Tiozzo et al., 2009). Previous studies show that deletion of *Wnt5a* leads to the thickening of the epithelium and mesenchyme in the embryonic lungs (Li et al., 2002). Moreover, *Wnt7b* is enriched in the lung epithelium (Shu et al., 2002), and loss of *Wnt7b* causes severe lung hypoplasia with reduced proliferation of the epithelium and mesenchyme (Rajagopal et al., 2008). We did not observe lung hypoplasia in *Sftpc-Cre; Wls^{loxp/loxp}* and *Nkx2.1-Cre; Wls^{loxp/loxp}* embryos, suggesting that *Wnt7b* likely exerts its function earlier than E10.5. In light of the distinctive phenotypes observed in the lungs of *Shh-Cre; Wls^{loxp/loxp}* and *Sftpc-Cre/Nkx2.1-Cre; Wls^{loxp/loxp}* mutants, *Wls* likely plays a different role before and after E10.5 during lung development.

Deletion of *Wls* with *Shh-Cre* alters the differentiation of lung progenitor cells (Cornett et al., 2013; Jiang et al., 2013). However, differentiation of airway progenitor cells seems unaffected in *Sftpc-Cre; Grp177^{loxp/loxp}* mutants (Fig. S2). Similar to the controls, *Sox2* is expressed in the airway epithelium (Fig. S2A), and the ratio of ciliated (*Foxj1*⁺), club cells (*Scgb1a1*⁺) and neuroendocrine (*Syp*⁺) is comparable with controls (Fig. S2A-D). That said, the numbers of AT2 cells per alveolar saccule are increased in *Sftpc-Cre; Wls^{loxp/loxp}* mutants at P30 (Fig. S2E), although the ratio of AT2 cells to alveolar *Nkx2.1*⁺ cells is unchanged ($81.49\% \pm 1.49\%$ Vs $84.95\% \pm 0.60\%$, $p = 0.0605$) (Fig. S2F). The transcript levels of *Sftpc* are also similar between mutants and littermate

controls (Fig. S2G). In addition, AT1 cells (Pdpn⁺) are normally distributed in the alveolar sacs of *Sftpc-Cre; Wls^{loxp/loxp}* mutants (Fig. S2C). These data indicate that *Wls* is required for epithelial differentiation prior to E10.5, and deletion of epithelial *Wls* after E10.5 has a limited impact on epithelial differentiation. Considering these distinct phenotypes, E9.5-E10.5 represents a unique stage in mouse lung development.

The persistent presence of α -SMA⁺ mesenchymal cells with increased collagen deposition in the alveoli following *Wls* deletion.

The transient presence of myofibroblasts is required for the formation of the secondary septae during neonatal alveologenesis (Branchfield et al., 2016). α -SMA⁺ myofibroblasts are rarely detected in the alveoli at P0. However, at P10 a significant number of myofibroblasts are present in the peripheral lungs, and these α -SMA⁺ cells are reduced to a minimal level at P30 (Fig. S3A). Remarkably, numerous α -SMA⁺ cells remain to form thick air sac walls in the alveoli of *Sftpc-Cre; Wls^{loxp/loxp}* and *Nkx2.1-Cre; Wls^{loxp/loxp}* mutants at P30 (Fig. 2A-D and S3A-D). Similar to the heterogeneous lung pathology observed in BPD patients (Thebaud et al., 2019), extensive numbers of Nkx2.1⁺ and SPC⁺ cells mixed with few myofibroblasts are also found in the high cell-density areas (Fig. S3D). The increased numbers of α -SMA⁺ cells in *Sftpc-Cre; Wls^{loxp/loxp}* mutants were confirmed by flow cytometry (FACS) analysis (8.76%±0.69% Vs 26.17%±1.78%, $p < 0.001$) (Fig. 2E, F and Fig. S4A). Consistently, the transcript and protein levels of α -SMA are increased in *Sftpc-Cre; Wls^{loxp/loxp}* mutants at P30 (Fig. 2G and H). Persistent α -SMA⁺ myofibroblasts produce and deposit ECM proteins including collagen and fibronectin in the alveoli as evidenced by Masson's trichrome staining (Fig. 2I). The transcript levels of *Colla1* and *Col3a1* are also increased in the mutant lungs (Fig. 2J). Taken together, these data support that deletion of epithelial *Wls* results in the persistent presence of α -SMA⁺ mesenchymal cells with increased collagen deposition within the alveoli.

Aberrant α -SMA expression in the alveolar endothelium of *Sftpc-Cre; Wls^{loxp/loxp}* mutants

Shh-Cre; Wls^{loxp/loxp} mutants show severe pulmonary hemorrhage due to abnormal vasculature (Cornett et al., 2013; Jiang et al., 2013). By contrast, pulmonary vasculature development seems normal in *Sftpc-Cre; Wls^{loxp/loxp}* mutants, as determined by the endothelial marker Endomucin at P10 (Fig. 3A). However, at P30 the ratio of lung endothelial cells among mesenchymal cells (CD45⁺EpCAM⁺) is significantly decreased in *Sftpc-Cre; Wls^{loxp/loxp}* mutants (51.53% \pm 0.32% Vs 23.23% \pm 0.77%, $p < 0.0001$) (Fig. 3B, C and Fig. S4B). Surprisingly, 9.44% \pm 0.27% endothelial cells co-express α -SMA in the alveoli, which were confirmed by immunostaining with the endothelial markers Pecam1 (CD31) and ERG (Fig. 3D and E). FACs analysis further reveals a dramatic increase of Pecam1⁺ α -SMA⁺ population in mutant lungs (1.34% \pm 0.09% Vs 0.14% \pm 0.01%, $p < 0.001$) (Fig. 3F, G and S4C). In addition, the transcript levels of the myofibroblast markers *Acta2* and *Tagln* are increased by about 7-fold in the isolated endothelial cells which also show a 4-fold increase of *Col1a1* and *Col3a1* (Fig. 3H). Reduced pulmonary microvessels have been reported in the enlarged air sac of BPD lungs (Bhatt et al., 2001). *Sftpc-Cre; Wls^{loxp/loxp}* mutant lungs also demonstrate enlarged air sacs with reduced numbers of endothelial cells. Interestingly, endothelial cells in the arteries of patients with pulmonary hypertension exhibit endothelial to mesenchymal transition (EndoMT), co-expressing α -SMA and endothelial markers Pecam1 and vWF (Good et al., 2015; Ranchoux et al., 2015). We also observed extensive Pecam1⁺ α -SMA⁺ endothelial cells in the mutant lungs. Hyperoxia exposure has been shown to reduce Pecam1 expression while promoting α -SMA expression in cultured human pulmonary microvascular endothelial cells (Zhang et al., 2018). Although it remains unknown whether Wnt signaling is involved in hyperoxia-associated EndoMT, our data support that Wnts from the epithelium are critical for endothelium differentiation in the developing lung.

Postnatal ablation of *Wls* causes abnormal α -SMA expression in the alveolar endothelium of *Ager-CreER*; *Wls*^{loxp/loxp} but not *Sftpc-CreER*; *Wls*^{loxp/loxp} mutants

To study whether *Wls* continues to play important roles in alveologenesis during early postnatal stage, *Sftpc-CreER*; *Wls*^{loxp/loxp} and *Ager-CreER*; *Wls*^{loxp/loxp} mice were administrated with tamoxifen at P2 and P10 to delete *Wls* in AT2 and AT1 cells, respectively (Fig. S5A and S6A). The *Sftpc-CreER* mouse line targets AT2 cells efficiently as ~99% of AT2 cells are labeled by the *Rosa26-tdtomato* reporter allele upon two doses of tamoxifen (Fig. S6B and C). Epithelial differentiation seems unperturbed in mutants with normal histology and differentiation of club, ciliated, AT1 and AT2 cells when examined at P30 (Fig. S5B, C and S6D, E). Although alveolar endothelial cells and myofibroblasts seem unaffected in *Sftpc-CreER*; *Wls*^{loxp/loxp} mutants (Fig. S6E), extensive α -SMA⁺ endothelial cells are present in the alveoli of *Ager-CreER*; *Wls*^{loxp/loxp} mutants (Fig. 3I). A recent study indicates that the *Ager-CreER* mouse line from the Jackson Laboratory targets the majority of AT1 and some AT2 cells (Penkala et al., 2021). Given normal endothelium development in *Sftpc-CreER*; *Wls*^{loxp/loxp} mutants, our results suggest that Wnts from AT1 cells are required for proper endothelial differentiation at the neonatal stage. Of note is that deletion of *Wls* in AT1 cells at E15.5 has minimal effects on alveologenesis when examined at P5 (Zepp et al., 2021), suggesting Wnts from AT1 cells are needed for mesenchymal differentiation at later stage of alveologenesis.

***Sftpc-Cre*; *Wls*^{loxp/loxp} mutants display exacerbated lung fibrosis upon bleomycin challenge.**

Neonatal hyperoxia causes permanent lung damage which renders the affected individuals more susceptible to environmental challenges (O'Reilly et al., 2008). Given that loss of epithelial *Wls* leads to persistent α -SMA⁺ mesenchymal cells, we asked whether *Sftpc-Cre*; *Wls*^{loxp/loxp} mutants display more severe pulmonary fibrosis following bleomycin challenge. Remarkably, fibrotic areas are significantly enlarged in mutants as compared to controls when examined at day14 after bleomycin treatment (Fig. 4A and B). Masson's Trichrome staining reveals extensive collagen deposition in the interstitial

space of mutant lungs (Fig. 4C). In consistence, α -SMA⁺ cells are enriched in the fibrotic foci of mutant lungs (Fig. 4D and E). These results suggest that *Sftpc-Cre; Wls^{loxp/loxp}* mutants are more susceptible to bleomycin challenge and that the persistent presence of alveolar α -SMA⁺ mesenchymal cells may serve as a source for fibrotic myofibroblasts during pulmonary fibrosis.

Wnt signaling plays a critical role in adult lung regeneration (Frank et al., 2016; Hogan et al., 2014; Kim et al., 2019; Nabhan et al., 2018; Tanjore et al., 2013; Zacharias et al., 2018). We therefore asked whether deletion of *Wls* in AT2 cells affects lung regeneration in *Sftpc-CreER; Wls^{loxp/loxp}* mice. We challenged the adult mutants with bleomycin after *Wls* ablation (Fig. S6F). Deletion of *Wls* prior to bleomycin treatment has minimal effects on lung regeneration, and the lung fibrotic area is comparable to controls (Fig. S6G and H). Masson's Trichome staining reveals a similar collagen deposition in the interstitial spaces (Fig. S6I). In addition, the numbers of myofibroblasts in the peripheral lungs are similar in mutants and controls (Fig. S6J and K). These findings are in contrast with the phenotypes observed in *Sftpc-Cre; Wls^{loxp/loxp}* mutants, suggesting that defective lungs beginning at an early postnatal state underlies worsening regeneration and fibrosis.

In conclusion, we demonstrate the essential role of epithelial Wnts in the formation of alveoli during the neonatal stage. Loss of *Wls* leads to abnormal differentiation of mesenchymal cells, resulting in the persistent presence of myofibroblasts and ectopic expression of α -SMA⁺ in the endothelial cells lining the enlarged air-sac. Our studies further suggest that Wnts produced by AT1 but not AT2 cells regulate endothelial differentiation at the early postnatal stage. This is consistent with the close proximity of AT1 cells and endothelium in the alveoli (Vila Ellis et al., 2020), and growth factors secreted by AT1 cells likely have direct impacts on pulmonary vasculature. Finally, in light of distinct phenotypes seen in *Shh-Cre; Wls^{loxp/loxp}* and *Sftpc-Cre; Wls^{loxp/loxp}* mutants, E9.5-E10.5 may represent a unique stage in mouse lung development.

Acknowledgements

We thank the colleagues in the Que laboratory for critical reading of the manuscript. This work is partly supported by R01HL152293, R01HL132996, R01HL158840 (to J.Q). Flow cytometry was performed in the Columbia Center for Translational Immunology (CCTI) Flow Cytometry Core at Columbia University Medical Center, supported in part by the Office of the Director, National Institutes of Health under the awards S10RR027050 and S10OD020056.

Materials and methods

Mice

The *Sftpc-Cre* (Okubo and Hogan, 2004), *Nkx2.1-Cre* (Xu et al., 2008), *Sftpc-CreER* (Rock et al., 2011), *Ager-CreER* (Jax #032771), *Axin2-lacZ* (Lustig et al., 2002) and *Wls^{loxp/loxp}* (Fu et al., 2011) mouse strains have been reported previously. For postnatal alveologenesis analysis, *Sftpc-Cre;Wls^{loxp/loxp}*, *Nkx2.1-Cre;Wls^{loxp/loxp}*, *Sftpc-CreER;Wls^{loxp/loxp}* and *Ager-CreER;Wls^{loxp/loxp}* mice are on C57BL/6 and 129/SvEv mixture background. For bleomycin treatment, *Sftpc-Cre;Wls^{loxp/loxp}* and *Sftpc-CreER;Wls^{loxp/loxp}* mice were backcrossed with C57BL/6 breeders for at least 6 generations. All mouse experiments and care were conducted in accordance with procedures approved by the Institutional Animal Care and Use Committee at Columbia University.

Tissue preparation and histology

Lung tissues were isolated after the mice were euthanized with isoflurane and fixed in 4% paraformaldehyde (PFA) overnight. Thick lung sections were performed as previously described (Branchfield et al., 2016). Briefly, 4% low-melt agarose was used for embedding whole lung lobes. 75 mm thickness sections were cut using a Leica vibratome. For paraffin section preparation, the tissues were dehydrated with ethanol and cleared in a

histoclear solution, and then embedded in paraffin. 7µm sections were cut and mounted on the slides for further histology staining and immunostaining. Hematoxylin and eosin (H&E) staining was performed as previously described (Fang et al., 2020; Jiang et al., 2021). Masson's Trichrome staining was performed by using commercial staining kit (Sigma, H15-1KT) according to the instruction. Nikon SMZ1500 Inverted microscope was used for obtaining images.

Immunofluorescence staining

Immunofluorescence staining was performed as previously described (Jiang et al., 2017). Briefly, the sections were deparaffinized and rehydrated. Following antigen retrieval with high-pressure heating in antigen unmasking solution (Vector Laboratory, H-3300) the sections were blocked with 5% normal donkey serum (Jackson ImmunoResearch Laboratories, 017-000-121) and then incubated with primary antibodies anti-Sox2 (Invitrogen, 14-9811-82, 1:200 dilution), anti-Foxj1 (Invitrogen, 14-9965-82, 1:100 dilution), anti-CC10 (Santa Cruz, sc-365992, 1:200 dilution), anti-SPC (Abcam, ab211326, 1:500 dilution), anti-Pdpn (DSHB, 8.1.1-c, 1:500 dilution), anti-αSMA (Sigma, A2547, 1:200 dilution), anti-SM22α (Abcam, ab14106, 1:200 dilution), anti-ERG (Abcam, ab92513, 1:200 dilution), anti-tdtomato (Biorbyt, orb182397, 1:1000 dilution), anti-Hopx (Santa Cruz, sc-398703, 1:100 dilution), anti-Endomucin (Santa Cruz, sc-65495, 1:200 dilution), anti-CD31 (BD, 550274, 1:100 dilution), anti-Synaptophysin (Abcam, ab32127, 1:200 dilution), anti-Ki67 (Cell Signaling Technology, 9129S, 1:200 dilution) and anti-TTF1 (Nkx2.1, Abcam, ab76013, 1:200 dilution) at 4°C overnight. Secondary antibodies (Jackson ImmunoResearch Laboratories) were added to the sections followed by extensive wash with PBS and incubation for 2 hours at room temperature. For TUNEL staining, In Situ Cell Death Detection Kit (Roche, 11684795910) was used according to the instructions. The nuclei were counterstained with DAPI, and images were obtained with Zeiss LSM T-PMT confocal laser-scanning microscope and analyzed by Zeiss software. For three-dimensional reconstructions, IMARIS software was used as previously described (Branchfield et al., 2016).

Isolation of lung endothelial cells and flow cytometry analysis

Single cell suspension was obtained from lung tissues as previously described (Dong et al., 2015), and the cells were incubated with fluorophore-conjugated antibodies CD45 (Biolegend, 103114, 1:100 dilution), EpCAM (Biolegend, 118212, 1:100 dilution) and CD31 (Biolegend, 102449, 1:100 dilution) in FACS buffer (5% FBS with 0.5 mM EDTA in PBS) 1 hour at 4°C, followed by incubation with the live/dead kit (Invitrogen, L34955) for 10 min at room temperature to exclude dead cells. To obtain lung endothelial cells, live CD45⁻EpCAM⁻CD31⁺ cells are gated and sorted. For FACS analysis, Foxp3/Transcription Factor Staining Buffer kit (eBioscience, 00-5523-00) was used for intracellular staining according to the instructions. The cells were then incubated with fluorophore-conjugated antibody against α -SMA (Invitrogen, 53-9760-82, 1:100 dilution) for 1 hour at room temperature. Data were obtained by using BD LSR II and analyzed with FlowJo software. Live CD45⁻EpCAM⁻ mesenchymal cells were gated for further analysis.

X-gal staining

X-gal staining was performed as previously described (Rodriguez et al., 2010). Briefly, lung tissues were dissociated and fixed with 4% PFA for 30 minutes at room temperature, and then the lungs were inflated with X-gal staining solution including 5 mM potassium ferrocyanide, 5 mM potassium ferricyanide, 50 mM MgCl₂, 0.5% NP-40 and 1 mg/mL X-gal and incubated at 37°C overnight. Lung tissues were post-fixed with 4% PFA for 2 hours at room temperature and dehydrated and embedded in paraffin for further sectioning as previously described (Que et al., 2007).

Western blotting

Western blotting analysis was performed as previously described (Jiang et al., 2013). Briefly, lung tissues were homogenized in Tris Buffer with the presence of the proteinase inhibitors cocktail (TissueLyser II). SDS-PAGE was used for separating mixed proteins

which were then transferred onto a polyvinylidene fluoride (PVDF) transfer membrane. Following blocking with 5% fat-free milk, the membrane was incubated in the primary antibodies anti- α -SMA (Sigma, 1:1000) and anti-GAPDH (ProteinTech, 1:5000) overnight at 4°C. The HRP-conjugated secondary antibody was used for assessing the expression of proteins.

RNA extraction and quantitative RT-PCR

Lung tissues were homogenized in Trizol buffer using TissueLyser II. Supernatants were obtained for total RNA extraction following centrifuging at 12,000 rpm for 10 min at 4°C. Total RNA was extracted according to instruction of commercial RNA extraction kit. The first-strand cDNA was synthesized from RNA by using SuperScript III First-Strand SuperMix kit. SYBR Green Supermix was used to quantify the cDNA by StepOnePlus Real-Time PCR System. The gene expression level was calculated relative to mouse β -actin by using the $2^{-\Delta(\Delta CT)}$ method. The sequences of qRT-PCR primers used in this study are described in Table S1.

Administration of tamoxifen and bleomycin

Tamoxifen was purchased from Sigma-Aldrich and dissolved in sunflower seed oil to 200 mg/mL for stock solution. The mice were intraperitoneally injected with tamoxifen at a dose of 200 mg/Kg every other day for total three doses. A phase period of ten days was used to wash out the residual tamoxifen before any further treatments. For bleomycin treatment, the 6-8 weeks old C57BL/6 background mice were anaesthetized by intraperitoneally injecting with tribromoethanol (Avertin) at a dose of 250 mg/Kg. Under anesthesia, the neck skin was opened to expose the trachea by blunt dissection, and bleomycin (Fresenius Kabi, USP) was delivered at a dose of 1.75 Unit/Kg body weight through intratracheal injection with a 30-Gauge needle. Samples were harvested for analysis at 14 days post bleomycin treatment.

Quantification and Statistical analysis

Measurement of mean linear intercept (MLI) was performed as previously described (Liu et al., 2017). For quantification of different types of epithelial cells and α -SMA⁺ cells, at least five random fields (20x magnification) were captured, and positive cells were counted using ImageJ software. At least three replicates were included for each group. All data are presented as the means \pm s.e.m. using GraphPad Prism 8. Unpaired two-tailed student's *t*-test was used to determine statistical significance. *p* values < 0.05 or less were considered statistically significant.

References

- Bellusci, S., Henderson, R., Winnier, G., Oikawa, T. and Hogan, B. L.** (1996). Evidence from normal expression and targeted misexpression that bone morphogenetic protein (Bmp-4) plays a role in mouse embryonic lung morphogenesis. *Development* **122**, 1693-1702.
- Bhatt, A. J., Pryhuber, G. S., Huyck, H., Watkins, R. H., Metlay, L. A. and Maniscalco, W. M.** (2001). Disrupted pulmonary vasculature and decreased vascular endothelial growth factor, Flt-1, and TIE-2 in human infants dying with bronchopulmonary dysplasia. *American journal of respiratory and critical care medicine* **164**, 1971-1980.
- Bostrom, H., Willetts, K., Pekny, M., Leveen, P., Lindahl, P., Hedstrand, H., Pekna, M., Hellstrom, M., Gebre-Medhin, S., Schalling, M., et al.** (1996). PDGF-A signaling is a critical event in lung alveolar myofibroblast development and alveogenesis. *Cell* **85**, 863-873.
- Bourbon, J., Boucherat, O., Chailley-Heu, B. and Delacourt, C.** (2005). Control mechanisms of lung alveolar development and their disorders in bronchopulmonary dysplasia. *Pediatric research* **57**, 38R-46R.
- Branchfield, K., Li, R., Lungova, V., Verheyden, J. M., McCulley, D. and Sun, X.** (2016). A three-dimensional study of alveologenesis in mouse lung. *Developmental biology* **409**, 429-441.
- Chao, C. M., Moiseenko, A., Zimmer, K. P. and Bellusci, S.** (2016). Alveologenesis: key cellular players and fibroblast growth factor 10 signaling. *Molecular and cellular pediatrics* **3**, 17.
- Colvin, J. S., White, A. C., Pratt, S. J. and Ornitz, D. M.** (2001). Lung hypoplasia and neonatal death in Fgf9-null mice identify this gene as an essential regulator of lung mesenchyme. *Development* **128**, 2095-2106.
- Cornett, B., Snowball, J., Varisco, B. M., Lang, R., Whitsett, J. and Sinner, D.** (2013). Wntless is required for peripheral lung differentiation and pulmonary vascular development. *Developmental biology* **379**, 38-52.

- Dong, Y., Geng, Y., Li, L., Li, X., Yan, X., Fang, Y., Li, X., Dong, S., Liu, X., Li, X., et al.** (2015). Blocking follistatin-like 1 attenuates bleomycin-induced pulmonary fibrosis in mice. *The Journal of experimental medicine* **212**, 235-252.
- Fang, Y., Liu, H., Huang, H., Li, H., Saqi, A., Qiang, L. and Que, J.** (2020). Distinct stem/progenitor cells proliferate to regenerate the trachea, intrapulmonary airways and alveoli in COVID-19 patients. *Cell research* **30**, 705-707.
- Frank, D. B., Peng, T., Zepp, J. A., Snitow, M., Vincent, T. L., Penkala, I. J., Cui, Z., Herriges, M. J., Morley, M. P., Zhou, S., et al.** (2016). Emergence of a Wave of Wnt Signaling that Regulates Lung Alveologenesis by Controlling Epithelial Self-Renewal and Differentiation. *Cell reports* **17**, 2312-2325.
- Fu, J., Ivy Yu, H. M., Maruyama, T., Mirando, A. J. and Hsu, W.** (2011). Gpr177/mouse Wntless is essential for Wnt-mediated craniofacial and brain development. *Developmental dynamics : an official publication of the American Association of Anatomists* **240**, 365-371.
- Good, R. B., Gilbane, A. J., Trinder, S. L., Denton, C. P., Coghlan, G., Abraham, D. J. and Holmes, A. M.** (2015). Endothelial to Mesenchymal Transition Contributes to Endothelial Dysfunction in Pulmonary Arterial Hypertension. *The American journal of pathology* **185**, 1850-1858.
- Goss, A. M., Tian, Y., Tsukiyama, T., Cohen, E. D., Zhou, D., Lu, M. M., Yamaguchi, T. P. and Morrissey, E. E.** (2009). Wnt2/2b and beta-catenin signaling are necessary and sufficient to specify lung progenitors in the foregut. *Developmental cell* **17**, 290-298.
- Harris-Johnson, K. S., Domyan, E. T., Vezina, C. M. and Sun, X.** (2009). beta-Catenin promotes respiratory progenitor identity in mouse foregut. *Proceedings of the National Academy of Sciences of the United States of America* **106**, 16287-16292.
- Hilgendorff, A. and O'Reilly, M. A.** (2015). Bronchopulmonary dysplasia early changes leading to long-term consequences. *Frontiers in medicine* **2**, 2.
- Hogan, B. L., Barkauskas, C. E., Chapman, H. A., Epstein, J. A., Jain, R., Hsia, C. C., Niklason, L., Calle, E., Le, A., Randell, S. H., et al.** (2014). Repair and regeneration of the respiratory system: complexity, plasticity, and mechanisms of lung stem cell function. *Cell stem cell* **15**, 123-138.
- Husain, A. N., Siddiqui, N. H. and Stocker, J. T.** (1998). Pathology of arrested acinar development in postsurfactant bronchopulmonary dysplasia. *Human pathology* **29**, 710-717.
- Jiang, M., Fang, Y., Li, Y., Huang, H., Wei, Z., Gao, X., Sung, H. K., Hu, J., Qiang, L., Ruan, J., et al.** (2021). VEGF receptor 2 (KDR) protects airways from mucus metaplasia through a Sox9-dependent pathway. *Developmental cell* **56**, 1646-1660 e1645.
- Jiang, M., Ku, W. Y., Fu, J., Offermanns, S., Hsu, W. and Que, J.** (2013). Gpr177 regulates pulmonary vasculature development. *Development* **140**, 3589-3594.
- Jiang, M., Li, H., Zhang, Y., Yang, Y., Lu, R., Liu, K., Lin, S., Lan, X., Wang, H., Wu, H., et al.** (2017). Transitional basal cells at the squamous-columnar junction generate Barrett's oesophagus. *Nature* **550**, 529-533.
- Jobe, A. H. and Bancalari, E.** (2001). Bronchopulmonary dysplasia. *American journal of respiratory and critical care medicine* **163**, 1723-1729.

- Kim, H. T., Yin, W., Nakamichi, Y., Panza, P., Grohmann, B., Buettner, C., Guenther, S., Ruppert, C., Kobayashi, Y., Guenther, A., et al. (2019).** WNT/RYK signaling restricts goblet cell differentiation during lung development and repair. *Proceedings of the National Academy of Sciences of the United States of America* **116**, 25697-25706.
- Kishimoto, K., Furukawa, K. T., Luz-Madrigal, A., Yamaoka, A., Matsuoka, C., Habu, M., Alev, C., Zorn, A. M. and Morimoto, M. (2020).** Bidirectional Wnt signaling between endoderm and mesoderm confers tracheal identity in mouse and human cells. *Nature communications* **11**, 4159.
- Li, C., Xiao, J., Hormi, K., Borok, Z. and Minoo, P. (2002).** Wnt5a participates in distal lung morphogenesis. *Developmental biology* **248**, 68-81.
- Lindahl, P., Karlsson, L., Hellstrom, M., Gebre-Medhin, S., Willetts, K., Heath, J. K. and Betsholtz, C. (1997).** Alveogenesis failure in PDGF-A-deficient mice is coupled to lack of distal spreading of alveolar smooth muscle cell progenitors during lung development. *Development* **124**, 3943-3953.
- Liu, Z., Fu, S. and Tang, N. (2017).** A Standardized Method for Measuring Internal Lung Surface Area via Mouse Pneumonectomy and Prosthesis Implantation. *Journal of visualized experiments : JoVE*.
- Lustig, B., Jerchow, B., Sachs, M., Weiler, S., Pietsch, T., Karsten, U., van de Wetering, M., Clevers, H., Schlag, P. M., Birchmeier, W., et al. (2002).** Negative feedback loop of Wnt signaling through upregulation of conductin/axin2 in colorectal and liver tumors. *Molecular and cellular biology* **22**, 1184-1193.
- McGowan, S. E., Grossmann, R. E., Kimani, P. W. and Holmes, A. J. (2008).** Platelet-derived growth factor receptor-alpha-expressing cells localize to the alveolar entry ring and have characteristics of myofibroblasts during pulmonary alveolar septal formation. *Anatomical record* **291**, 1649-1661.
- Mucenski, M. L., Wert, S. E., Nation, J. M., Loudy, D. E., Huelsken, J., Birchmeier, W., Morrissey, E. E. and Whitsett, J. A. (2003).** beta-Catenin is required for specification of proximal/distal cell fate during lung morphogenesis. *The Journal of biological chemistry* **278**, 40231-40238.
- Mund, S. I., Stampanoni, M. and Schittny, J. C. (2008).** Developmental alveolarization of the mouse lung. *Developmental dynamics : an official publication of the American Association of Anatomists* **237**, 2108-2116.
- Nabhan, A. N., Brownfield, D. G., Harbury, P. B., Krasnow, M. A. and Desai, T. J. (2018).** Single-cell Wnt signaling niches maintain stemness of alveolar type 2 cells. *Science* **359**, 1118-1123.
- Northway, W. H., Jr., Rosan, R. C. and Porter, D. Y. (1967).** Pulmonary disease following respirator therapy of hyaline-membrane disease. Bronchopulmonary dysplasia. *The New England journal of medicine* **276**, 357-368.
- O'Reilly, M. A., Marr, S. H., Yee, M., McGrath-Morrow, S. A. and Lawrence, B. P. (2008).** Neonatal hyperoxia enhances the inflammatory response in adult mice infected with influenza A virus. *American journal of respiratory and critical care medicine* **177**, 1103-1110.
- Okubo, T. and Hogan, B. L. (2004).** Hyperactive Wnt signaling changes the developmental potential of embryonic lung endoderm. *Journal of biology* **3**, 11.

- Penkala, I. J., Liberti, D. C., Pankin, J., Sivakumar, A., Kremp, M. M., Jayachandran, S., Katzen, J., Leach, J. P., Windmueller, R., Stolz, K., et al. (2021). Age-dependent alveolar epithelial plasticity orchestrates lung homeostasis and regeneration. *Cell stem cell* **28**, 1775-1789 e1775.
- Que, J., Okubo, T., Goldenring, J. R., Nam, K. T., Kurotani, R., Morrissey, E. E., Taranova, O., Pevny, L. H. and Hogan, B. L. (2007). Multiple dose-dependent roles for Sox2 in the patterning and differentiation of anterior foregut endoderm. *Development* **134**, 2521-2531.
- Rajagopal, J., Carroll, T. J., Guseh, J. S., Bores, S. A., Blank, L. J., Anderson, W. J., Yu, J., Zhou, Q., McMahon, A. P. and Melton, D. A. (2008). Wnt7b stimulates embryonic lung growth by coordinately increasing the replication of epithelium and mesenchyme. *Development* **135**, 1625-1634.
- Ranchoux, B., Antigny, F., Rucker-Martin, C., Hautefort, A., Pechoux, C., Bogaard, H. J., Dorfmueller, P., Remy, S., Lecerf, F., Plante, S., et al. (2015). Endothelial-to-mesenchymal transition in pulmonary hypertension. *Circulation* **131**, 1006-1018.
- Rock, J. R., Barkauskas, C. E., Cronic, M. J., Xue, Y., Harris, J. R., Liang, J., Noble, P. W. and Hogan, B. L. (2011). Multiple stromal populations contribute to pulmonary fibrosis without evidence for epithelial to mesenchymal transition. *Proceedings of the National Academy of Sciences of the United States of America* **108**, E1475-1483.
- Rodriguez, P., Da Silva, S., Oxburgh, L., Wang, F., Hogan, B. L. and Que, J. (2010). BMP signaling in the development of the mouse esophagus and forestomach. *Development* **137**, 4171-4176.
- Schittny, J. C., Mund, S. I. and Stamanoni, M. (2008). Evidence and structural mechanism for late lung alveolarization. *American journal of physiology. Lung cellular and molecular physiology* **294**, L246-254.
- Shu, W., Guttentag, S., Wang, Z., Andl, T., Ballard, P., Lu, M. M., Piccolo, S., Birchmeier, W., Whitsett, J. A., Millar, S. E., et al. (2005). Wnt/beta-catenin signaling acts upstream of N-myc, BMP4, and FGF signaling to regulate proximal-distal patterning in the lung. *Developmental biology* **283**, 226-239.
- Shu, W., Jiang, Y. Q., Lu, M. M. and Morrissey, E. E. (2002). Wnt7b regulates mesenchymal proliferation and vascular development in the lung. *Development* **129**, 4831-4842.
- Snowball, J., Ambalavanan, M., Cornett, B., Lang, R., Whitsett, J. and Sinner, D. (2015). Mesenchymal Wnt signaling promotes formation of sternum and thoracic body wall. *Developmental biology* **401**, 264-275.
- Tanjore, H., Degryse, A. L., Crossno, P. F., Xu, X. C., McConaha, M. E., Jones, B. R., Polosukhin, V. V., Bryant, A. J., Cheng, D. S., Newcomb, D. C., et al. (2013). beta-catenin in the alveolar epithelium protects from lung fibrosis after intratracheal bleomycin. *American journal of respiratory and critical care medicine* **187**, 630-639.
- Thebaud, B., Goss, K. N., Laughon, M., Whitsett, J. A., Abman, S. H., Steinhorn, R. H., Aschner, J. L., Davis, P. G., McGrath-Morrow, S. A., Soll, R. F., et al. (2019). Bronchopulmonary dysplasia. *Nature reviews. Disease primers* **5**, 78.

- Tiozzo, C., De Langhe, S., Yu, M., Londhe, V. A., Carraro, G., Li, M., Li, C., Xing, Y., Anderson, S., Borok, Z., et al.** (2009). Deletion of Pten expands lung epithelial progenitor pools and confers resistance to airway injury. *American journal of respiratory and critical care medicine* **180**, 701-712.
- Vila Ellis, L., Cain, M. P., Hutchison, V., Flodby, P., Crandall, E. D., Borok, Z., Zhou, B., Ostrin, E. J., Wythe, J. D. and Chen, J.** (2020). Epithelial Vegfa Specifies a Distinct Endothelial Population in the Mouse Lung. *Developmental cell* **52**, 617-630 e616.
- Xu, Q., Tam, M. and Anderson, S. A.** (2008). Fate mapping Nkx2.1-lineage cells in the mouse telencephalon. *The Journal of comparative neurology* **506**, 16-29.
- Yang, J., Hernandez, B. J., Martinez Alanis, D., Narvaez del Pilar, O., Vila-Ellis, L., Akiyama, H., Evans, S. E., Ostrin, E. J. and Chen, J.** (2016). The development and plasticity of alveolar type 1 cells. *Development* **143**, 54-65.
- Yin, Y., White, A. C., Huh, S. H., Hilton, M. J., Kanazawa, H., Long, F. and Ornitz, D. M.** (2008). An FGF-WNT gene regulatory network controls lung mesenchyme development. *Developmental biology* **319**, 426-436.
- Zacharias, W. J., Frank, D. B., Zepp, J. A., Morley, M. P., Alkhaleel, F. A., Kong, J., Zhou, S., Cantu, E. and Morrissey, E. E.** (2018). Regeneration of the lung alveolus by an evolutionarily conserved epithelial progenitor. *Nature* **555**, 251-255.
- Zepp, J. A., Morley, M. P., Loebel, C., Kremp, M. M., Chaudhry, F. N., Basil, M. C., Leach, J. P., Liberti, D. C., Niethamer, T. K., Ying, Y., et al.** (2021). Genomic, epigenomic, and biophysical cues controlling the emergence of the lung alveolus. *Science* **371**.
- Zhang, K., Yao, E., Lin, C., Chou, Y. T., Wong, J., Li, J., Wolters, P. J. and Chuang, P. T.** (2020). A mammalian Wnt5a-Ror2-Vangl2 axis controls the cytoskeleton and confers cellular properties required for alveologenesis. *eLife* **9**.
- Zhang, Y., Dong, X., Shirazi, J., Gleghorn, J. P. and Lingappan, K.** (2018). Pulmonary endothelial cells exhibit sexual dimorphism in their response to hyperoxia. *American journal of physiology. Heart and circulatory physiology* **315**, H1287-H1292.

Figures

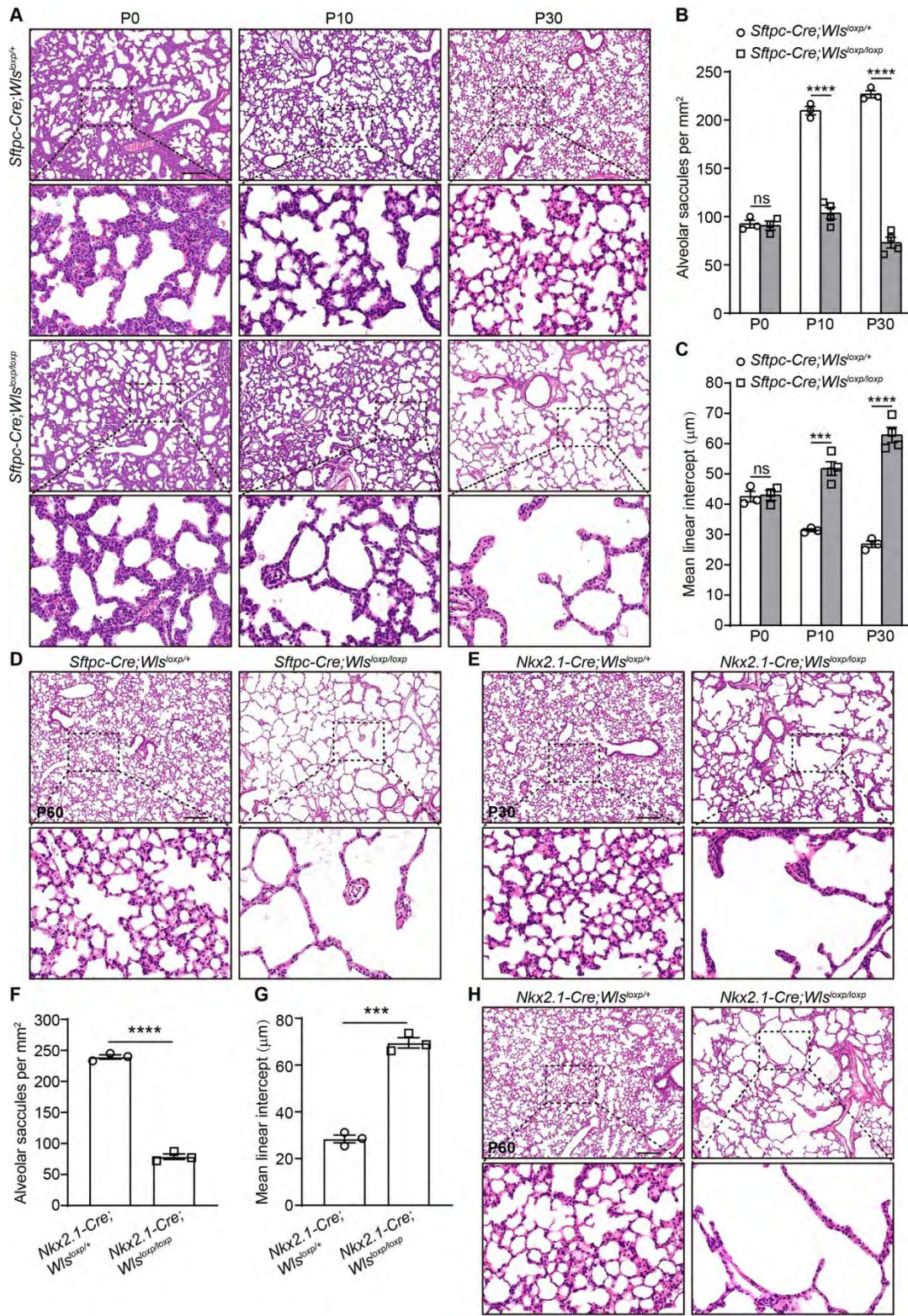


Figure 1. Loss of lung epithelial *Wls* leads to BPD-like emphysema.

(A) Hematoxylin and Eosin (H&E) staining of lung sections from *Sftpc-Cre; Wls^{loxp/loxp}* mutants and control mice at different postnatal days. (B) The saccule numbers of *Sftpc-Cre; Wls^{loxp/loxp}* mutants and control mice were quantified at different postnatal days. (C) The mean linear intercept (MLI) values of *Sftpc-Cre; Wls^{loxp/loxp}* mutants and control mice were measured at different postnatal days. (D) H&E staining of lung sections from *Sftpc-Cre; Wls^{loxp/loxp}* mutants and control mice at postnatal (P) day 60. (E) H&E staining of lung sections from *Nkx2.1-Cre; Wls^{loxp/loxp}* mutants and control mice at P30. (F) The saccule numbers of *Nkx2.1-Cre; Wls^{loxp/loxp}* mutants and control mice were quantified at P30. (G) The MLI values of *Nkx2.1-Cre; Wls^{loxp/loxp}* mutants and control mice were measured at P30. (H) H&E staining of lung sections from *Nkx2.1-Cre; Wls^{loxp/loxp}* mutants and control mice at P60. n = 3. ***, $p < 0.001$; ****, $p < 0.0001$. Scale bar: 200 μm .

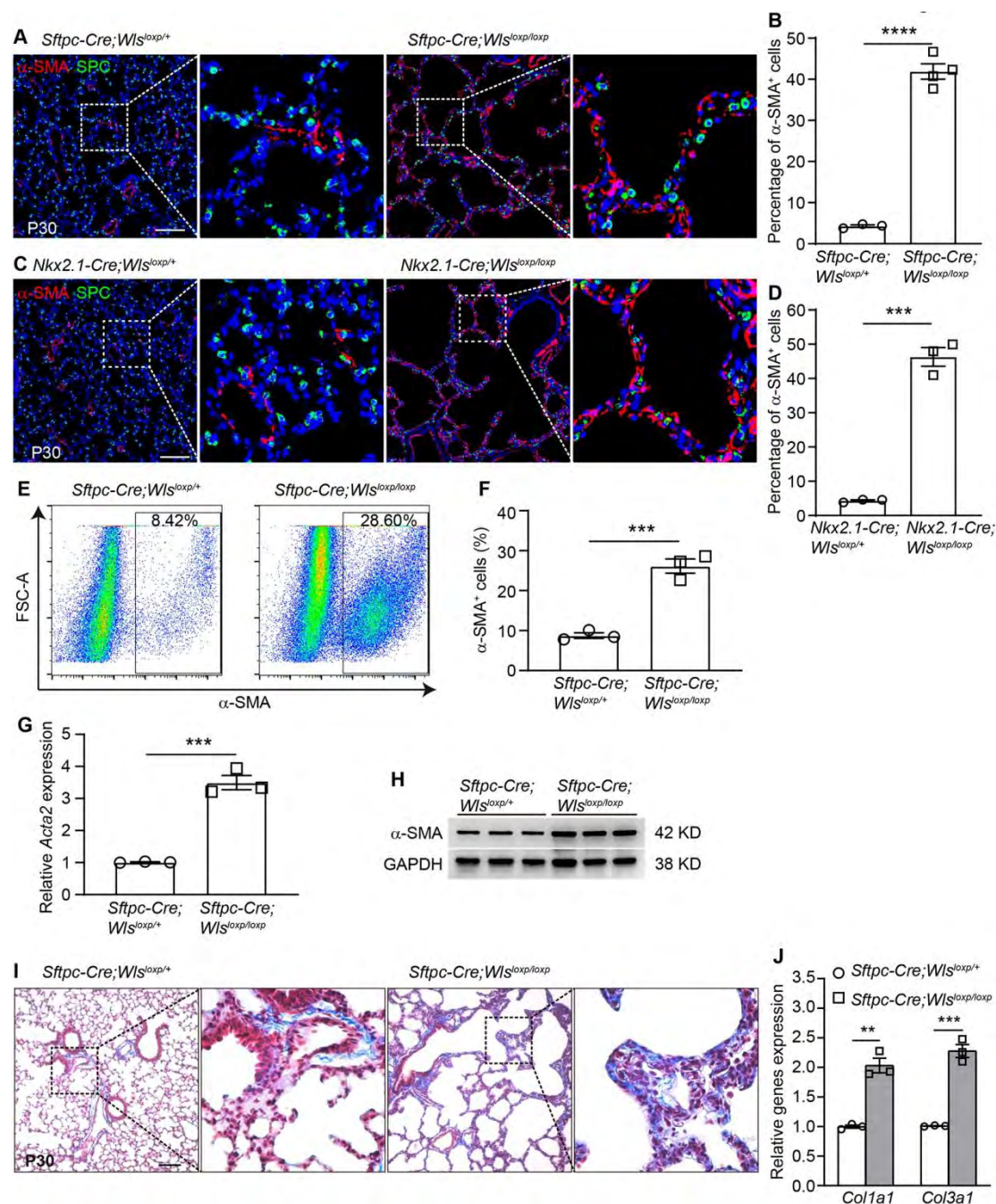


Figure 2. Deletion of lung epithelial *Wls* leads to the persistent presence of alveolar α -SMA⁺ mesenchymal cells and collagen deposition.

(A) Immunofluorescence analysis of α -SMA and SPC in lung sections from *Sftpc-Cre; Wls^{loxp/loxp}* mutants and control mice at P30. (B) Quantification of alveolar α -SMA⁺ cells

in the lungs of *Sftpc-Cre*; *Wls*^{loxp/loxp} mutants and control mice at P30. (C) Immunofluorescence analysis of α -SMA and SPC in lung sections from *Nkx2.1-Cre*; *Wls*^{loxp/loxp} mutants and control mice at P30. (D) Quantification of alveolar α -SMA⁺ cells of *Nkx2.1-Cre*; *Wls*^{loxp/loxp} mutants and control mice at P30. (E) Flow cytometry analysis of α -SMA⁺ cells among CD45⁻ EpCAM⁻ mesenchymal cells in lung tissues isolated from *Sftpc-Cre*; *Wls*^{loxp/loxp} mutants and control mice at P30. (F) Quantification of the ratio of α -SMA⁺ cells to CD45⁻ EpCAM⁻ mesenchymal cells. (G) qRT-PCR analysis of *Acta2* in lung tissues from *Sftpc-Cre*; *Wls*^{loxp/loxp} mutants and control mice. (H) Western blot analysis of α -SMA in lung tissues isolated from *Sftpc-Cre*; *Wls*^{loxp/loxp} mutants and control mice. GAPDH was used as a loading control. (I) Masson's trichrome staining of lung sections from *Sftpc-Cre*; *Wls*^{loxp/loxp} mutants and control mice at P30. (J) qRT-PCR analysis of *Colla1* and *Col3a1* in lung tissues isolated from *Sftpc-Cre*; *Wls*^{loxp/loxp} mutants and control mice. n = 3; **, $p < 0.01$; ***, $p < 0.001$; ****, $p < 0.0001$. Scale bar: 100 μ m.

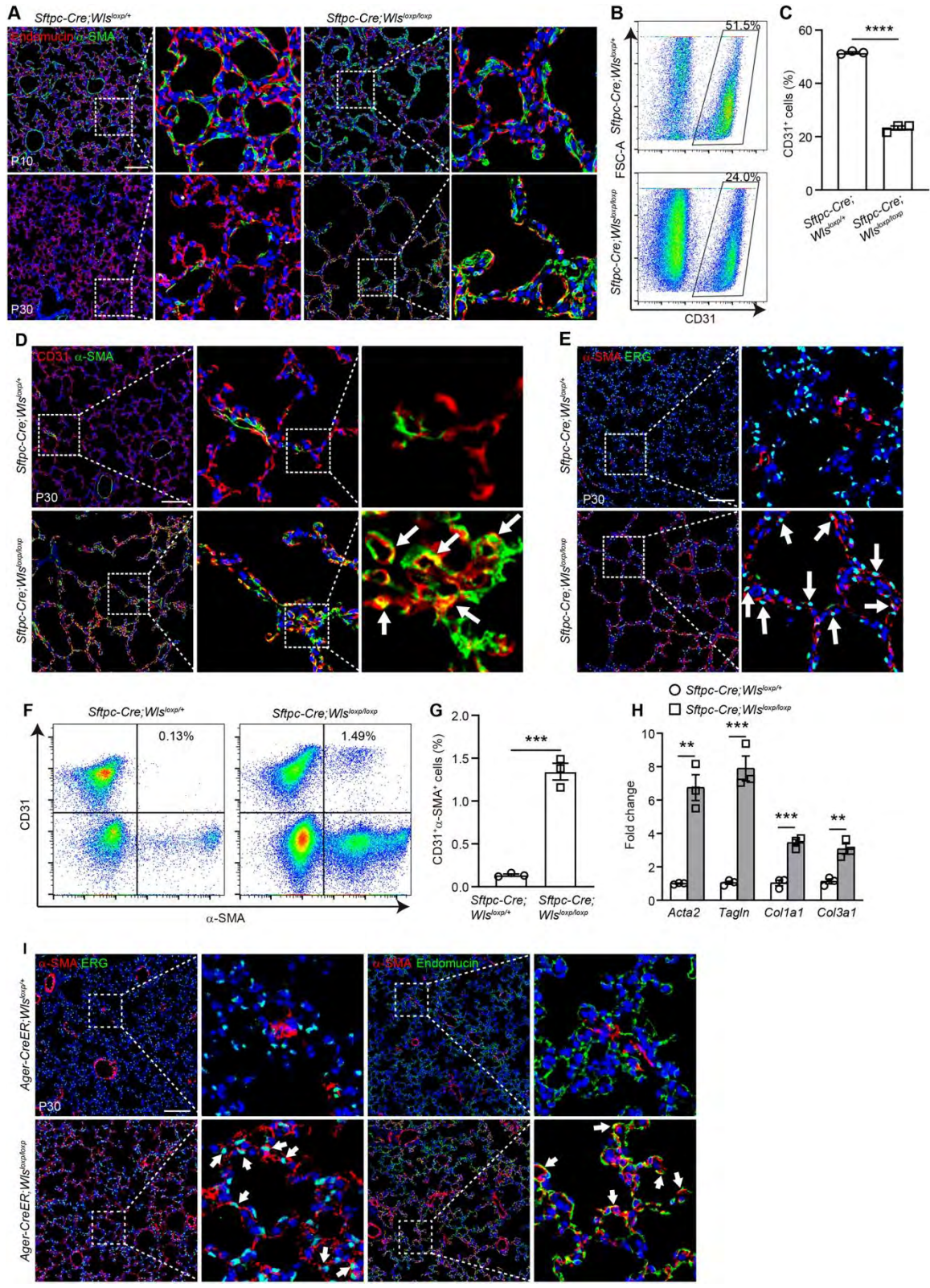


Figure 3. Aberrant α -SMA expression in the pulmonary endothelium of *Sftpc-Cre*; *Wls^{loxp/loxp}* and *Ager-CreER*; *Wls^{loxp/loxp}* mutants.

(A) Immunofluorescence analysis of α -SMA and Endomucin in lung sections of *Sftpc-Cre*; *Wls^{loxp/loxp}* mutants and control mice at P10 and P30. (B) Flow cytometry analysis of CD31⁺ cells in CD45⁻EpCAM⁻ mesenchymal cells in lung tissues isolated from *Sftpc-Cre*; *Wls^{loxp/loxp}* mutants and control mice at P30. (C) Quantification of the ratio of CD31⁺ cells to CD45⁻EpCAM⁻ mesenchymal cells. (D) Immunofluorescence analysis of α -SMA and CD31 in lung sections isolated from *Sftpc-Cre*; *Wls^{loxp/loxp}* and control mice at P30. (E) Immunofluorescence analysis of α -SMA and ERG in lung sections isolated from *Sftpc-Cre*; *Wls^{loxp/loxp}* and control mice at P30. (F) Flow cytometry analysis of α -SMA and CD31 in lung tissues isolated from *Sftpc-Cre*; *Wls^{loxp/loxp}* mutants and control mice at P30. (G) Quantification of the proportion of CD31⁺ α -SMA⁺ cells in CD45⁻EpCAM⁻ mesenchymal cells. (H) qRT-PCR analysis of *Acta2*, *Tagln*, *Colla1* and *Col3a1* transcripts in the lung epithelium isolated from *Sftpc-Cre*; *Wls^{loxp/loxp}* mutants and control mice at P30. (I) Immunofluorescence analysis of α -SMA, ERG and Endomucin in lung sections from *Ager-CreER*; *Wls^{loxp/loxp}* and control mice at P30. n = 3; **, $p < 0.01$; ***, $p < 0.001$; ****, $p < 0.0001$. Scale bar: 100 μ m.

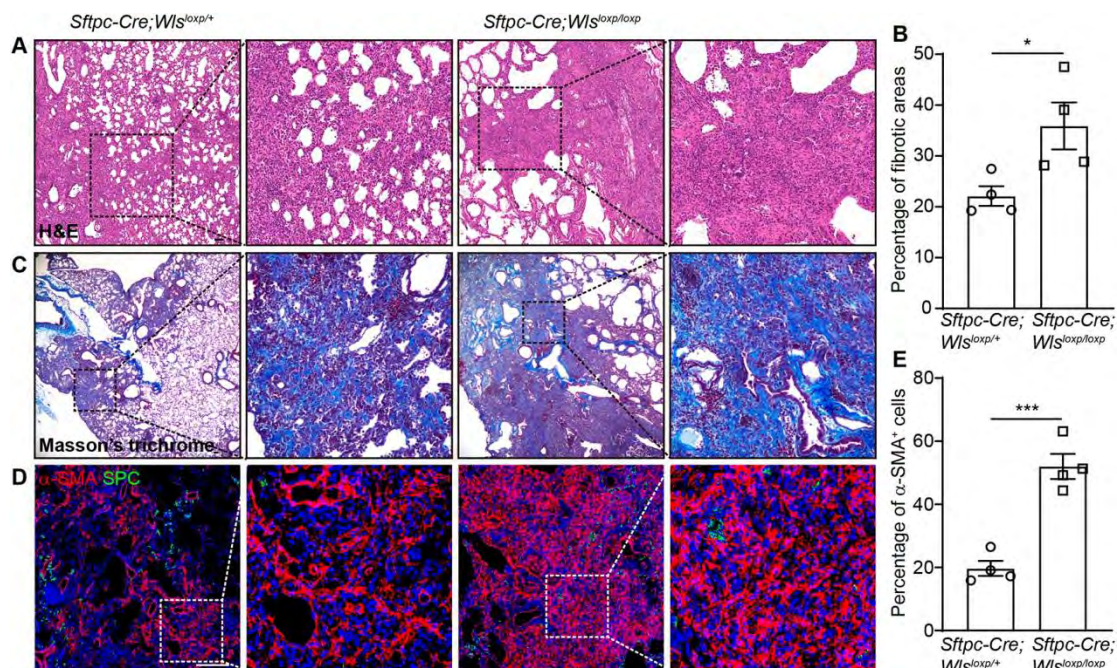


Figure 4. *Sftpc-Cre; Wls^{loxp/loxp}* mutants display exacerbated lung fibrosis upon bleomycin challenge.

(A) H&E staining of lung sections from *Sftpc-Cre; Wls^{loxp/loxp}* mutants and control mice 14 days post bleomycin treatment. (B) Quantification of fibrotic areas in the lungs of *Sftpc-Cre; Wls^{loxp/loxp}* mutants and control mice 14 days post bleomycin treatment. (C) Masson's trichrome staining of lung sections of *Sftpc-Cre; Wls^{loxp/loxp}* mutants and control mice 14 days post bleomycin treatment. (D) Immunofluorescence analysis of α -SMA and SPC in lung sections of *Sftpc-Cre; Wls^{loxp/loxp}* mutants and control mice 14 days post bleomycin challenge. (E) Quantification of α -SMA⁺ cells of *Sftpc-Cre; Wls^{loxp/loxp}* mutants and control mice 14 days post bleomycin treatment. n = 4, *, $p < 0.05$; ***, $p < 0.001$. Scale bar: 100 μ m.

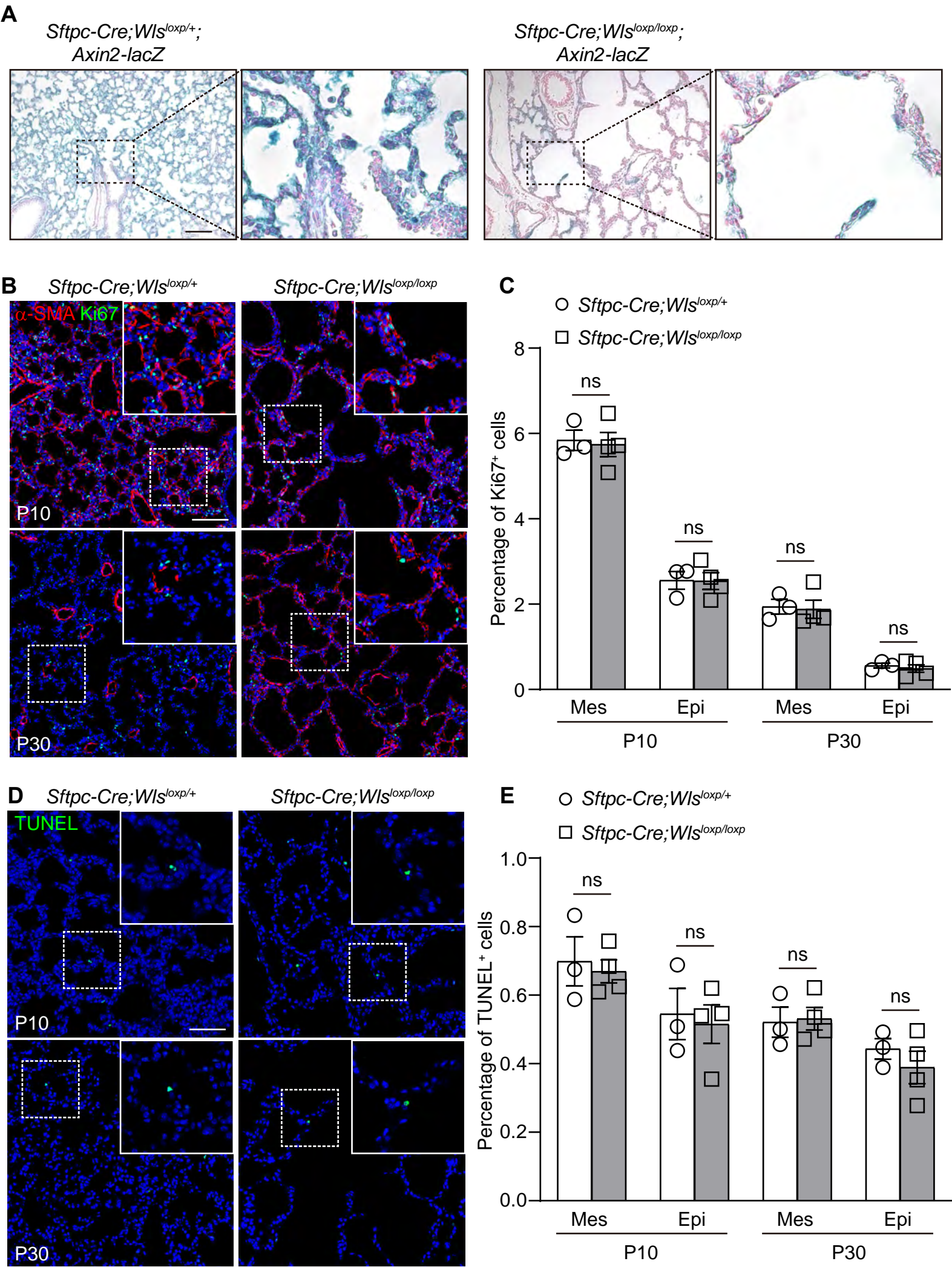


Fig. S1. Wnt signaling suppression does not affect cell proliferation and apoptosis in the lungs of *Sftpc-Cre*; *Wls^{loxp/loxp}* mutants.

(A) X-gal staining of lung tissues from *Sftpc-Cre*; *Wls^{loxp/+}*; *Axin2-lacZ* and *Sftpc-Cre*; *Wls^{loxp/loxp}*; *Axin2-lacZ* mice at P30. (B) Immunofluorescence analysis of α -SMA and Ki67 in lung sections from *Sftpc-Cre*; *Wls^{loxp/loxp}* mutants and control mice at P10 and P30. (C) Quantification of Ki67⁺ mesenchymal and epithelial cells in the lungs of *Sftpc-Cre*; *Wls^{loxp/loxp}* mutants and control mice at P10 and P30. (D) TUNEL staining of lung sections from *Sftpc-Cre*; *Wls^{loxp/loxp}* mutants and control mice at P10 and P30. (E) Quantification of TUNEL⁺ cells in the lung mesenchyme and epithelium of *Sftpc-Cre*; *Wls^{loxp/loxp}* mutants and control mice at P10 and P30. Mes: Mesenchyme, Epi: Epithelium, n = 3. ns, non-significant. Scale bar: 100 μ m.

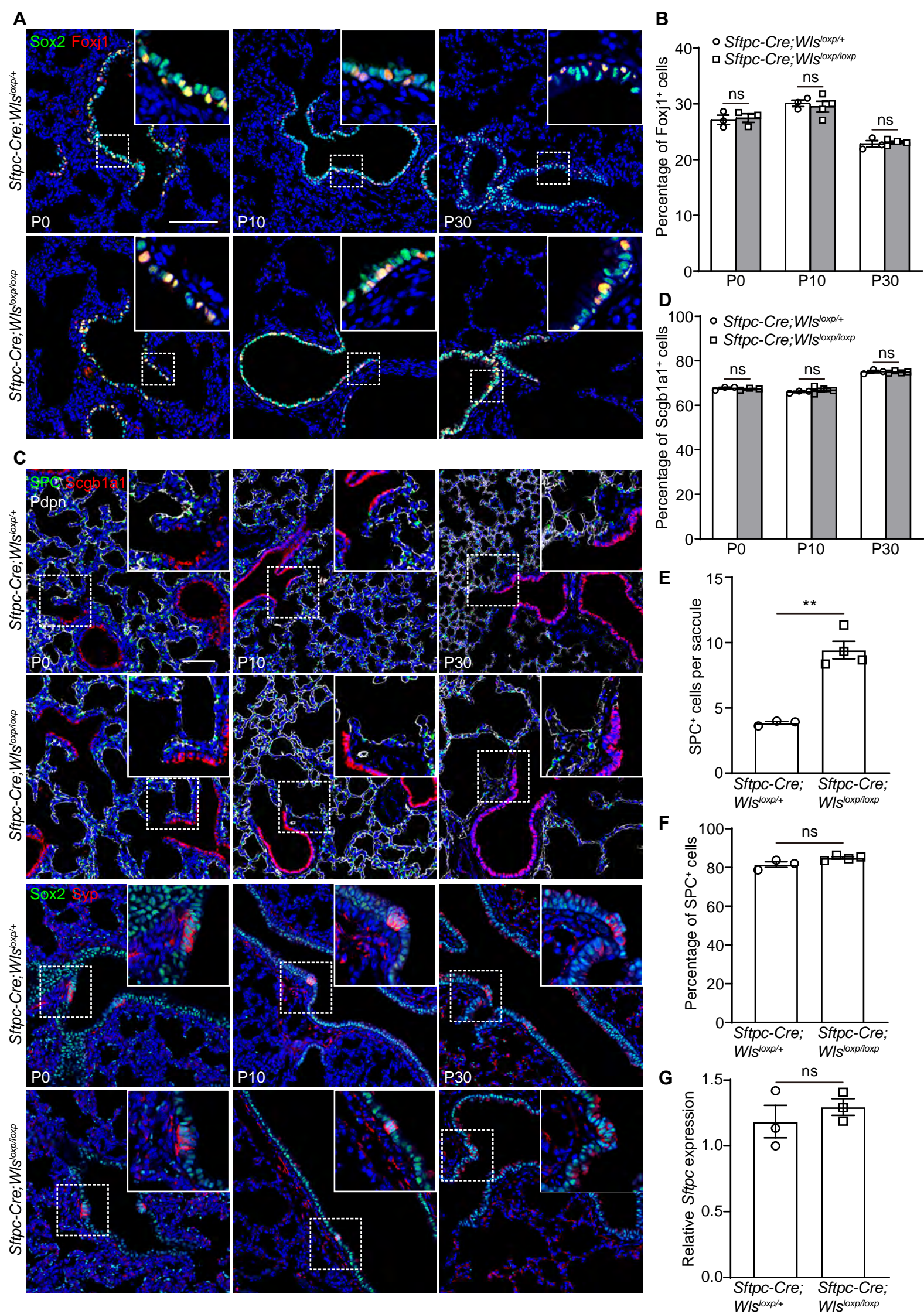


Fig. S2. Loss of epithelial Wls has minimal effects on epithelial differentiation in the lungs of *Sftpc-Cre; Wls^{loxp/loxp}* mutants.

(A-B) The ratio of ciliated cell (Foxj1⁺) to airway epithelium (Sox2⁺) in *Sftpc-Cre; Wls^{loxp/loxp}* mutants. (C) Immunofluorescence analysis of club cells (Scgb1a1⁺), alveolar type 2 (AT2, SPC⁺) cells, alveolar type 1 (AT1, Pdpn⁺) cells and neuroendocrine cells (Syp⁺) in the lung of *Sftpc-Cre; Wls^{loxp/loxp}* mutants and control mice. (D) The ratio of club cell to airway epithelium in the lungs of *Sftpc-Cre; Wls^{loxp/loxp}* mutants and control mice. (E) Quantification of SPC⁺ cells per saccule in the lungs of *Sftpc-Cre; Wls^{loxp/loxp}* mutants and control mice at P30. (F) Quantification of SPC⁺ cells in alveolar Nkx2.1⁺ cells of *Sftpc-Cre; Wls^{loxp/loxp}* mutants and control mice at P30. (G) The transcript levels of *Sftpc* in lung tissues from *Sftpc-Cre; Wls^{loxp/loxp}* mutants and control mice measured by qRT-PCR. n = 3. **, *p* < 0.01. ns, not significant. Scale bar: 100 μm.

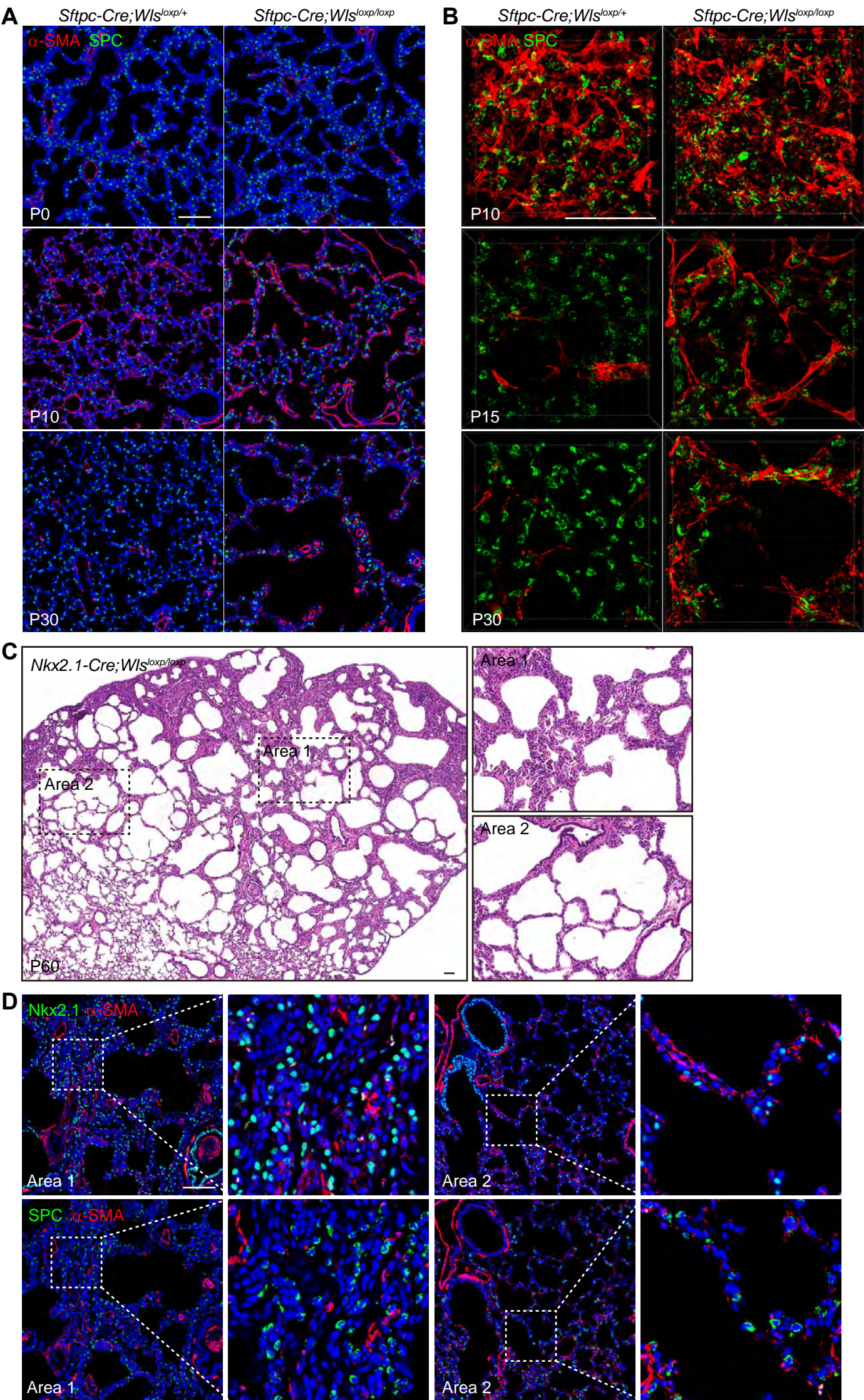


Fig. S3. Deletion of lung epithelial *Wls* results in enlarged air sacs with the persistent presence of α -SMA⁺ mesenchymal cells.

(**A-B**) Immunofluorescence analysis of α -SMA and SPC in the lungs of *Sftpc-Cre; Wls^{loxp/loxp}* mutants and control mice at various postnatal days. Note 2-dimension images (**A**) and 3-dimension reconstruction images (**B**). (**C**) H&E staining of lung sections from *Nkx2.1-Cre; Wls^{loxp/loxp}* mutants and control mice at P60. (**D**) Immunofluorescence analysis of α -SMA, Nkx2.1 and SPC in the lungs of *Nkx2.1-Cre; Wls^{loxp/loxp}* mutants and control mice at P30. Scale bar: 100 μ m.

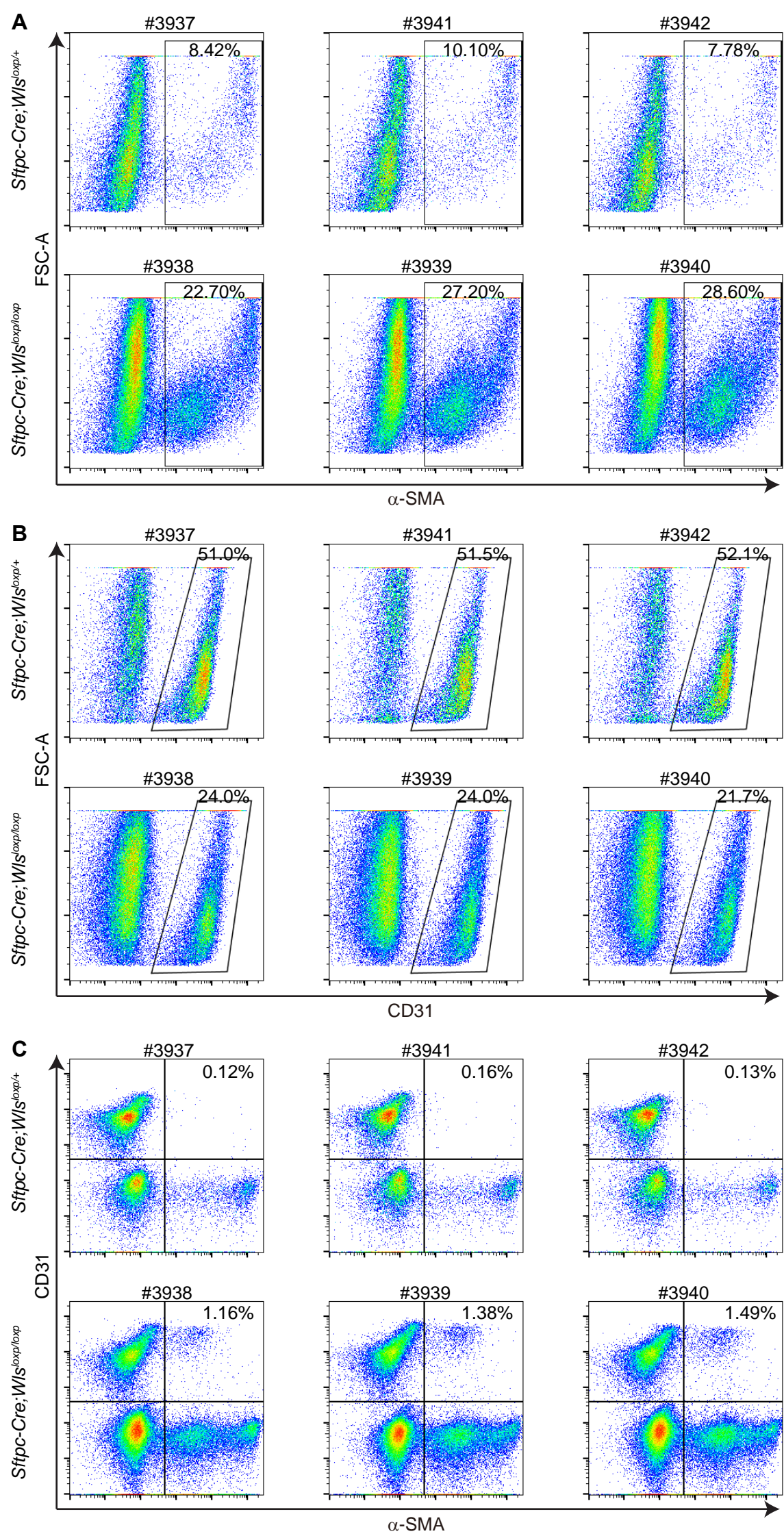


Fig. S4. Flow cytometry analysis of CD31 and α -SMA.

FACS analysis to show the ratio of (A) α -SMA⁺ cells, (B) CD31⁺ cells or (C) α -SMA⁺CD31⁺ cells in CD45⁻ EpCAM⁻ lung mesenchymal cells. Cells were isolated from *Sftpc-Cre; Wls^{loxp/loxp}* mutants and control mice at P30. n=3 for each group, and individual FACS images are presented.

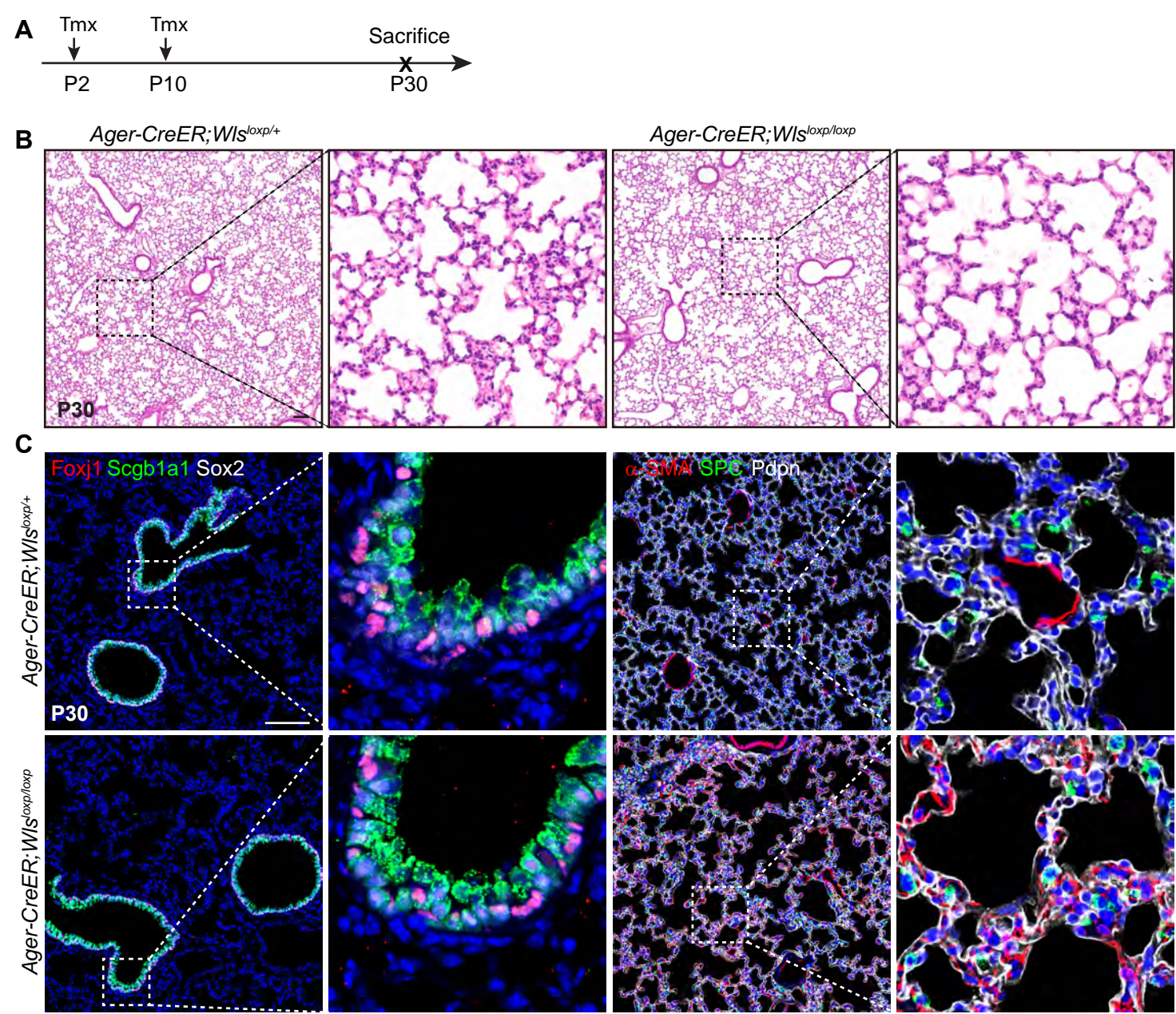


Fig. S5. Aberrant alveolar α-SMA⁺ endothelial cells in *Ager-CreER; Wls^{loxp/loxp}* mutants

(A) Schematic diagram depicts the timing of tamoxifen injection at the neonatal stage. Tmx: tamoxifen. (B) H&E staining of the lung section from *Ager-CreER; Wls^{loxp/loxp}* mutants and control mice at P30. (C) Immunofluorescence analysis of Scgb1a1⁺ club cells, Foxj1⁺ ciliated cells, SPC⁺ AT2 cells, Pdpn⁺ AT1 cells and α-SMA⁺ cells in the lungs of *Ager-CreER; Wls^{loxp/loxp}* mutants and control mice. Scale bar: 100 μm. Note that this *Ager-CreER* mouse line was purchased from the Jackson Laboratory (Jax #032771), and labels the majority of AT1 cells and 10%-20% AT2 cells at P2-P5 and ~50% AT2 cells in adult (Penkala et al., 2021). The original *Ager-CreER* mouse line labels a minimal number (1%-3%) of AT2 cells at late embryonic stage and adult (Chung and Hogan, 2018).

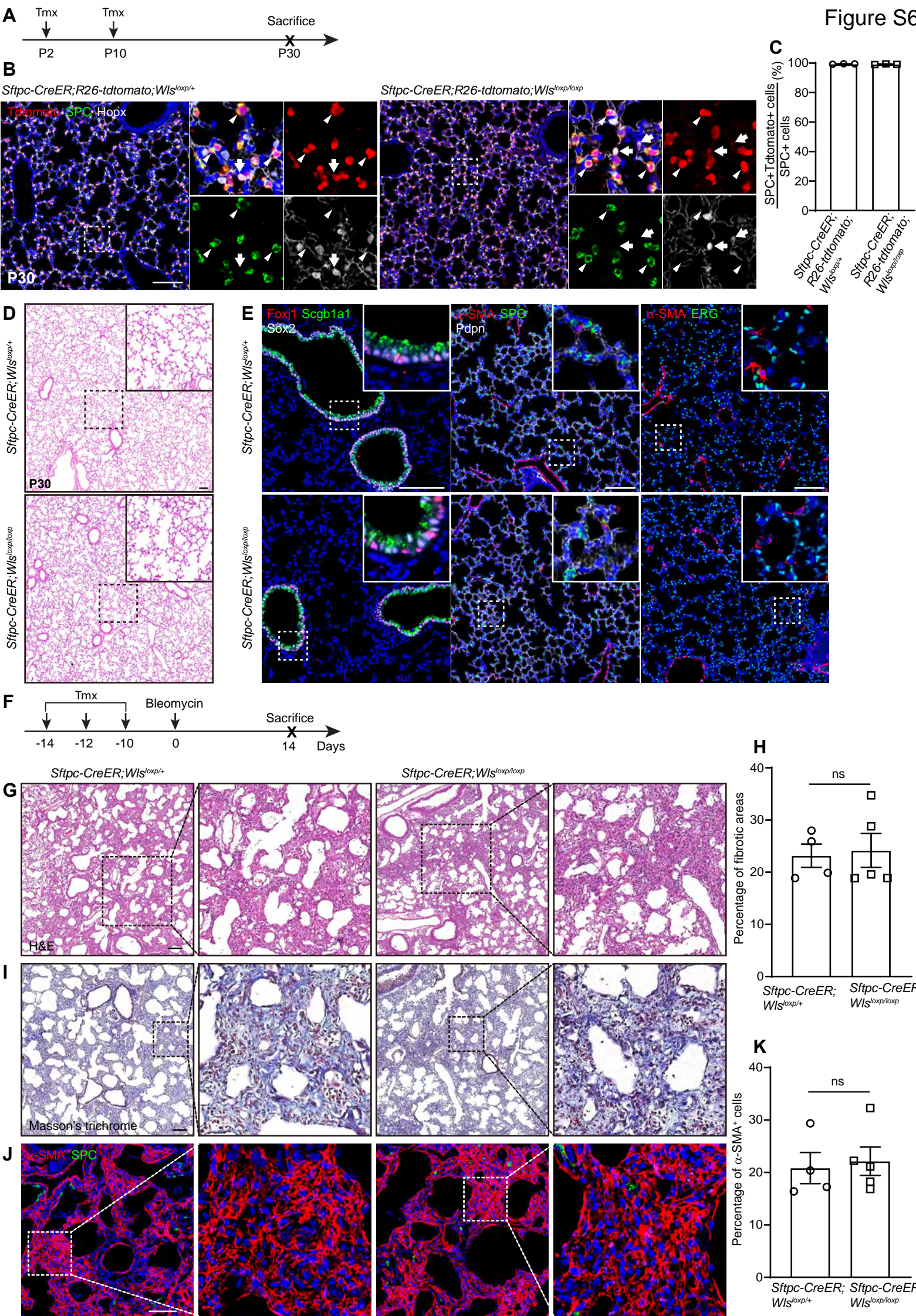


Fig. S6. Ablation of *Wls* in adult AT2 cells has minimal effects on pulmonary fibrosis upon bleomycin challenge.

(A) Schematic diagram for the timing of tamoxifen injection. Tmx: tamoxifen. (B) Lineage tracing analysis of AT2 cells as revealed by anti-Tdtomato and SPC at P30. (C) Quantification of lineage-labeled AT2 cells from *Sftpc-CreER; R26-tdtomato; Wls^{loxp/+}* and *Sftpc-CreER; R26-tdtomato; Wls^{loxp/loxp}* mice. (D) Histology of the lungs isolated from *Sftpc-CreER; Wls^{loxp/loxp}* and control mice at P30. (E) Immunofluorescence analysis of Scgb1a1⁺ club cells, Foxj1⁺ ciliated cells, SPC⁺ AT2 cells, Pdpn⁺ AT1 cells, α -SMA⁺ cells and ERG⁺ endothelial cells in the lungs of *Sftpc-CreER; Wls^{loxp/loxp}* mutants and control mice at P30. (F) Schematic diagram for the timing of tamoxifen injection and bleomycin challenge. (G) H&E staining of lung sections from *Sftpc-CreER; Wls^{loxp/loxp}* and control mice 14 days post bleomycin challenge. (H) Quantification of fibrotic areas in the lungs of *Sftpc-CreER; Wls^{loxp/loxp}* and control mice 14 days post bleomycin treatment. (I) Masson's trichrome staining of lung sections of *Sftpc-CreER; Wls^{loxp/loxp}* and control mice 14 days post bleomycin challenge. (J) Immunofluorescence analysis of α -SMA and SPC in lung sections of *Sftpc-CreER; Wls^{loxp/loxp}* and control mice 14 days post bleomycin challenge. (K) Quantification of α -SMA⁺ cells in the lungs of *Sftpc-CreER; Wls^{loxp/loxp}* mutants and control mice 14 days post bleomycin treatment. n = 4, ns: not significant. Scale bar: 100 μ m.

Table S1. The sequences of qRT-PCR primers

Genes	Forward primers_sequences	Reverse primers_sequences
b-actin	ACCTTCTACAATGAGCTGCG	CCTGGATAGCAACGTACATGG
Acta2	GTGAAGAGGAAGACAGCACAG	GCCCATTCCAACCATTACTCC
Tagln	CCAGACTGTTGACCTCTATGAAG	TCTTATGCTCCTGGGCTTTC
Colla1	CATAAAGGGTCATCGTGGCT	TTGAGTCCGTCTTTGCCAG
Col3a1	GAAGTCTCTGAAGCTGATGGG	TTGCCTTGCGTGTTTGATATTC
Sftpc	TTGTCGTGGTGATTGTAGGG	TGGAAAAGGTAGCGATGGTG